MR IMAGES SEGMENTATION AND BIAS CORRECTION VIA LIC MODEL

Lingfeng Wang[1,2]*, Jie Huang*[2]*, Bin Lai*[3]*, and Chunhong Pan*[2]

1. Hunan Provincial Key Laboratory of Network Investigational Technology, Hunan Police Academy
2. NLPR, Institute of Automation, Chinese Academy of Sciences, 3. Agricultural Bank of China

ABSTRACT

This paper presents a novel Linear Intrinsic Component (LIC) model for simultaneous estimation of bias field and segmentation of magnetic resonance (MR) images with the intensity inhomogeneity. The core of LIC model is linear transformation, which is derived from Taylor expansion of non-linear model. Due to the linear transformation, observed image can be decomposed into four components, namely, true image, which characterizes a physical property of the tissues, multiplicative and additive bias fields, which result in intensity inhomogeneity, and Gaussian noises. Based on sub-space constraint on two bias fields, and piecewise smoothness restriction on the true image, we can performing the task of joint bias field estimation and image segmentation. To model the complex noises subject to non-gaussian distribution, we further extend LIC model by introducing the non-gaussian noise term, and propose the Non-Gaussian LIC (NGLIC) model. By adopting L_1 regularization to our solution, the NGLIC model can be effectively solved by iterative soft-thresholding approach. Both LIC and NGLIC models are evaluated on a lot of MR simulated images downloaded from BrainWeb and real images, showing the superiority to the state-of-the-art approach on both segmentation and bias field correction results.

Index Terms— Image Segmentation, Bias Correction, Linear Intrinsic Component

1. INTRODUCTION

Magnetic resonance (MR) image segmentation is a fundamental issue in medical image processing, and provides essential information for clinic diagnosis, therapeutic scheme and treatment monitoring. However, MR images always suffer from intensity inhomogeneities and complex noises. To solve these difficulties, a large number of methods have been proposed.

One of the classical method is the M-S model proposed in [1, 2, 3]. In [4, 5], Chan and Vese proposed the CV model. Unfortunately, the CV model is not able to solve the intensity inhomogeneity problem. To solve this problem, Li *et al.* introduced the local binary fitting (LBF) model in [6], as well as the followers, i.e., [7, 8, 9, 10, 11, 12, 13, 14]. However, these methods can not gain the bias field explicitly. Accordingly, in [15], Li *et al.* proposed a variational level set approach for simultaneous segmentation and bias correction. The main problem of this model is that the distribution of different tissues are assumed to be the same. For this problem, Zhang *et al.* in [16] developed a statistical and variational multiphase method on the basis of the method in [15]. By adding parameters to adjust the variance differences among different tissues, the model can obtain more accurate segmentation and bias field correction results. In [17], Wang *et al.* introduced a fixed smooth regularization implemented by the gradient operation. Specifically, it forces the smoothness of bias field through minimizing the gradient of bias field.

The above methods are implemented under level set framework. The main limitation is that level set implementation heavily depends on the initialization of the segmented contour. To solve this problem, Li *et al.* [18] proposed a method named multiplicative intrinsic component optimization (MICO). In this model, the bias field is considered as a linear combination of a set of smooth basis functions. Motivated by this method, In [19], rough-sets are integrated with intensity represented by stomped normal(SN) distribution. In [20], Xie *et al.* proposed a modified Markov Random Field (MRF) segmentation method with an interleaved structure. Improved performances, including bias field correction and image segmentation results, have been reported by comparing with the other methods. Unfortunately, in their papers, the bias field is only considered as a multiplicative component. In practice, the generating mechanism of bias field is very complex, even non-linear of the true or intrinsic image. The key issue addressed in this paper is to propose a new bias field model, and develop a new simultaneous bias field estimation and image segmentation method based on this model.

In this paper, we propose a new model to joint bias field estimation and image segmentation. To model the sophisticated-origin intensity inhomogeneity, we introduce a non-linear mapping function to represent the observed image, which is a non-linear transformation of the intrinsic image. To make it solvable, the non-linear mapping is approximated with a linear mapping by introducing the Taylor expansion technique. Based on the linear transformation, the observed image is decomposed into four components except the noise term, namely, the true image, the multiplicative bias field and the additive bias field. Bias field estimation and tissue segmentation are simultaneously achieved by an energy minimization process, aimed to optimize the estimates of these three components of an MR image. To model complex noises, we propose the new non-Gaussian LIC (NGLIC) model. In this model, the L_1 regularization is adopted to restrict the non-Gaussian noise term. As a result, the NGLIC model is effectively solved by iterative soft-thresholding way.

Specifically, the main contributions and details of this paper are highlighted as follows:

1) The novel LIC model is proposed in this paper. As a result, the sophisticated-origin intensity inhomogeneity is modeled by introducing both multiplicative and additive bias fields. Owing to the new formulation of intensity inhomogeneity, our model can obtain better bias correction and image segmentation results.

2) To consider complex noises, the LIC model is further extended to NGLIC model by introducing the non-Gaussian term. Owing to the introduction of the non-Gaussian term, NGLIC model is more

This work is supported by the National Natural Science Foundation of China (Grant No. 61403376 and 91646207), the Youth Innovation Promotion Association CAS, the Beijing Nature Science Foundation (Grant No. 4162064), and the Open Research Fund of Hunan Provincial Key Laboratory of Network Investigational Technology (Grant No. 2015HNWLFZ055).

robust to complex noises as compared with the LIC model as well as the state-of-the-art approach.

2. LINEAR INTRINSIC COMPONENT MODEL

MR images ubiquitously suffer from sophisticated-origin inhomogeneities, leading to a tough task of tissue segmentation. To model the inhomogeneities, the acquired or observed image $I \in \mathbb{R}^d$ is considered as a complicated non-linear transformation of the intrinsic image $J \in \mathbb{R}^d$, given by[1]

$$I = f(J) + n, \tag{1}$$

where $f(.)$ is the non-linear transformation of mapping function, and n is the Gaussian noise. It is hard to directly formulate the non-linear mapping function into image segmentation or bias correction task. For this reason, we utilize Taylor expansion to approximate the non-linear mapping function f, that is,

$$f(J) = f(J_0) + f'(J_0)(J - J_0) + o(J - J_0), \tag{2}$$

where J_0 is the Taylor expansion point, $f'(J_0)$ is the first-derivative of $f(.)$, and $o(J - J_0)$ represents high-order error of this expansion. By ignoring high-order terms, Eqn. (1) can be reformulated as

$$f(J) = Jf'(J_0) + f(J_0) - J_0 f'(J_0). \tag{3}$$

By defining $b = f'(J_0) \in \mathbb{R}^d$ and $a = f(J_0) - J_0 f'(J_0) \in \mathbb{R}^d$, Eqn. (1) can be reformulated as

$$I = b \odot J + a + n, \tag{4}$$

where $\odot$ is the Hadamard operation which represents multiplication of corresponding elements.

As illustrated in Eq. (4), the observed image I is generated by a linear transformation of the intrinsic image J with two parameters , b and a. Thereby, the proposed simultaneous image segmentation and bias correction model is named linear intrinsic component (LIC) model. Parameters b and a are considered as multiplicative and additive bias fields, respectively.

2.1. Intrinsic Image and Bias Fields Representation

The Intrinsic Image is assumed to be partitioned into N parts $\{\Omega_i\}_{i=1}^N$, satisfying that

$$\cup_{i=1}^N \Omega_i = \Omega, \;\; \Omega_i \cap \Omega_j = \varnothing, \; \forall i \neq j,$$

where Ω is the image domain. The intensities of the i-th part Ω_i are assumed to be a constant c_i. Hence, the intrinsic image is

$$J = \sum_{i=1}^{N} c_i u_i, \tag{5}$$

where $u_i \in \mathbb{R}^d$ is the i-th membership function, indicating the i-th part. The definition of u_i is

$$u_i(x) = \begin{cases} 1, & x \in \Omega_i \\ 0, & \text{otherwise} \end{cases},$$

in which $x \in \Omega$ is the location of a pixel or voxel.

[1]Each image is reshaped as a vector with the dimension to be d.

The Multiplicative and Additive Bias Fields are assumed to be spatially smooth. To describe this characteristic, each bias field is approximated by a linear combination of a set of smooth basis functions, that is, the multiplicative and additive bias fields are

$$b = G^T \boldsymbol{w} = \sum_{i=1}^{M} w_i g_i, \text{ and } a = G^T \boldsymbol{v} = \sum_{i=1}^{M} v_i g_i, \tag{6}$$

where $g_i \in \mathbb{R}^d$ is the i-th basis, and $G = (g_1, g_2, \ldots, g_M)^T$ is the basis matrix. $\boldsymbol{w} = (w_1, w_2, \ldots, w_M)^T$ and $\boldsymbol{v} = (v_1, v_2, \ldots, v_M)^T$ are two weighting vectors. Same with [18], we use 10 polynomials of the first two degrees as the basis functions.

2.2. Energy function and Optimization

According to the LIC model in Eq. (4), the simultaneous image segmentation and bias field correction is able to be formulated as the following minimizing problem

$$\min_{b,J,a} \|I - b \odot J - a\|_2^2 . \tag{7}$$

Combining Eqs. (5) and (6), we reformulate Eq. (7) as

$$\min_{\{c_i,u_i\}_{i=1}^N, \boldsymbol{w}, \boldsymbol{v}} \mathcal{F}\left(\{c_i, u_i\}_{i=1}^N, \boldsymbol{w}, \boldsymbol{v}\right), \tag{8}$$

where

$$\mathcal{F}\left(\{c_i, u_i\}_{i=1}^N, \boldsymbol{w}, \boldsymbol{v}\right) = \left\| I - G^T \boldsymbol{w} \odot \sum_{i=1}^{N} c_i u_i - G^T \boldsymbol{v} \right\|_2^2 . \tag{9}$$

By considering that $u_i^T u_j = 0, \; \forall i \neq j$; $\sum_{i=1}^N u_i = \mathbf{1}$, where $\mathbf{1}$ is a vector with all elements are 1s, Eq. (9) can be converted into

$$\mathcal{F}(\{c_i, u_i\}_{i=1}^N, \boldsymbol{w}, \boldsymbol{v}) = \sum_{i=1}^{N} \left\| \left(I - G^T \boldsymbol{w} c_i - G^T \boldsymbol{v} \right) \odot u_i \right\|_2^2 . \tag{10}$$

Eq. (10) is the object function of the LIC model. In the following, we will describe the optimization method in detail.

2.3. Optimization Eq. (10)

The alternating optimization method [21] is adopted to solve Eq. (10) in the following three steps:

Optimizing $\{c_i\}_{i=1}^N$: Fixing $\boldsymbol{w}$, $\boldsymbol{v}$, and $\{u_i\}_{i=1}^N$, we then minimize the energy function by setting $\frac{\partial \mathcal{F}}{\partial c_i} = 0, \; \forall i = 1, 2, ..., N$. Parameters $\{c_i\}_{i=1}^N$ are estimated by

$$\hat{c}_i = \frac{w^T G \left(\left(I - G^T v \right) \odot u_i \right)}{w^T G \left(G^T w \odot u_i \right)}, \; i = 1, 2, ..., N. \tag{11}$$

Optimizing $\{u_i\}_{i=1}^N$: As for N segmentation parts (kinds of tissues), at each pixel or voxel x, there are N square distance results when the other parameters are available; namely,

$$\delta_i(x) = \left\| I(x) - G^T \boldsymbol{w}(x) c_i - G^T \boldsymbol{v}(x) \right\|_2^2, \; i = 1, 2, ..., N. \tag{12}$$

The voxel or pixel x is classified as certain segmentation part by minimum $\{\delta_i\}_{i=1}^N$. As a result, the parameters $\{u_i\}_{i=1}^N$ is able to be calculated by

$$u_i(x) = \begin{cases} 1, & i = \text{argmin}_i \, \delta_i(x) \\ 0, & \text{Otherwise} \end{cases} . \tag{13}$$

Optimizing $\boldsymbol{w}$ and $\boldsymbol{v}$: Fixing $\boldsymbol{v}$, $\{c_i\}_{i=1}^N$, and $\{u_i\}_{i=1}^N$, the parameter $\boldsymbol{w}$ is calculated by

$$\hat{\boldsymbol{w}} = \left(\sum_{i=1}^{N}\left(Gu_i{u_i}^T G^T c_i^2\right)\right)^{-1}\left(\sum_{i=1}^{N}\left(G\left(I - G^T\boldsymbol{v}\right)\odot c_i u_i\right)\right). \tag{14}$$

Similarly, the parameter $\boldsymbol{v}$ is calculated by

$$\hat{\boldsymbol{v}} = \left(GG^T\right)^{-1}\left(\sum_{i=1}^{N}\left(G\left(I - G^T\boldsymbol{w}c_i\right)\odot u_i\right)\right). \tag{15}$$

2.4. Implementation

The implementation progress of LIC model is that:

STEP_1: Initializing all of the parameters: $b = \mathbf{1}$, $a = \mathbf{0}$, c_i and u_i are set randomly;

STEP_2: Optimizing c_i by Eq. (11);

STEP_3: Optimizing u_i by Eq. (13);

STEP_4: Optimizing $\boldsymbol{w}$ by Eq. (14);

STEP_5: Optimizing $\boldsymbol{v}$ by Eq. (15).

STEP_6: Repeating **STEP_2**, **STEP_3**, **STEP_4** and **STEP_5** until the maximum number of iteration is reached. Same with [18], we set the maximum number of iteration to be a value of 20.

3. EXTENSION OF NON-GAUSSIAN NOISES

In the LIC model, the noise is assumed as Gaussian. However, in practice, the noises are complex which are always subject to non-Gaussian format, such as salt&pepper noise and laplacian noise. To address this problem, we extend the LIC model by introducing the non-Gaussian term, given by

$$I = f(J) + e + n, \tag{16}$$

where vector $e \in \mathbb{R}^d$ is the non-Gaussian noise term. The new model is named non-Gaussian LIC (NGLIC) model.

Motivated by [22], the non-Gaussian noise is assumed to be Laplacian noise. In such a case, the objective function of the NGLIC model $\mathcal{F}(\{c_i, u_i\}_{i=1}^N, \boldsymbol{w}, \boldsymbol{v}, e)$ is defined as

$$\frac{1}{2}\left\|I - G^T\boldsymbol{w}\odot\sum_{i=1}^{N}c_i u_i - G^T\boldsymbol{v} - e\right\|_2^2 + \lambda\left\|e\right\|_1, \tag{17}$$

where λ is a positive weighting value of the 1-norm term.

Energy function minimization is solved in the same iterative way as the LIC model. Therefore, the optimizations of $\{c_i\}_{i=1}^N$,$\{u_i\}_{i=1}^N$, $\boldsymbol{w}$ and $\boldsymbol{v}$ of the NGLIC model are same with the LIC model. Given $\{c_i\}_{i=1}^N$,$\{u_i\}_{i=1}^N$, $\boldsymbol{w}$ and $\boldsymbol{v}$, the non-Gaussian term e is optimized by using the soft-thresholding technique, given by

$$\hat{e}(x) = S_\lambda\left(I(x) - G^T\boldsymbol{w}(x)\sum_{i=1}^{N}c_i u_i - G^T\boldsymbol{v}(x)\right), \tag{18}$$

where $S_\lambda(x) = \max(|x| - \lambda, 0)$. Please refer to [22] for the details about the Laplacian noise and soft-thresholding technique.

4. EXPERIMENT RESULTS

In this section, both qualitative and quantitative methods are utilized to evaluate the proposed LIC and NGLIC models by comparing with the recent MICO model proposed in [18]. In the following, we first present details about the datasets and evaluation criteria. Then, we present comparative results on both synthetic and real images.

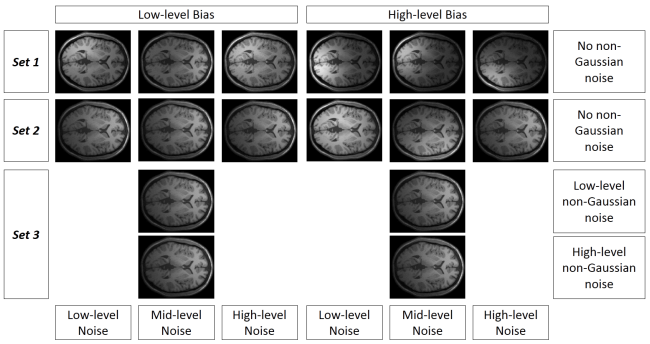

Fig. 1. Datasets generation schematic.

Table 1. Factors considered in dataset generation.

Set No.	Bias Type	M-bias	A-bias	NG-noise	G-noise
Set 1	Gaussian	$\surd$			$\surd$
Set 2	Gaussian	$\surd$	$\surd$		$\surd$
Set 3	Gaussian	$\surd$	$\surd$	$\surd$	$\surd$

4.1. Datasets and Evaluation criteria

For quantitative comparisons, the testing images are downloaded from the website of BrainWeb[2]. For each image, we add different types of bias, including multiplicative bias (M-bias) and additive bias (A-bias), and different types of noise, including Gaussian noise (G-noise) and Salt&Pepper noise (NG-noise). As illustrated in Table 1, we generate 3 different sets. For example, in *Set 1*, the images are blurred by the M-bias and G-noise.

There are 2 levels of bias intensities, 3 levels of gaussian noise intensities, and 2 levels of non-Gaussian intensities. For example, in *Set 1*, 2 levels of bias and 3 levels of Gaussian noise make up six kinds of simulation composition. *Set 2* is the same as *Set 1*, except that the bias levels are both applied to the multiplicative and additive biases. In *Set 3*, we fix the Gaussian noise level and adopt 2 levels of bias and 2 levels of non-Gaussian noise, so that there are four kinds of composition. The visual results are shown in Fig. 1.

We adopt F-score and CJV as criteria to evaluate the performances of image segmentation and bias correction results, respectively. As for the segmentation results, classification accuracy is calculated by F-score over the whole image at pixel-level, given by,

$$\text{F-score} = \frac{2\cdot\text{TP}}{2\cdot\text{TP}+\text{FN}+\text{FP}} = \frac{2\cdot\mathcal{R}_s\cap\mathcal{R}_g}{\mathcal{R}_s\cap\mathcal{R}_g+\mathcal{R}_s\cup\mathcal{R}_g}, \tag{19}$$

where TP, FP and FN represent true positives, false positives and false negatives, respectively; $\mathcal{R}_s$ is the region obtained by the segmentation algorithm and $\mathcal{R}_g$ is the corresponding ground truth. A good algorithm should provide a large F-score value.

As for the evaluation of bias field correction performance, we employ coefficient of joint variance (CJV), which is measured by statistic of gray matter (GM) and white matter (WM), given by,

$$\text{CJV} = \frac{\sigma(\text{GM})+\sigma(\text{WM})}{|\mu(\text{GM})-\mu(\text{WM})|}, \tag{20}$$

where σ and μ represent standard deviation and mean value of certain tissue, like GM or WM. To solve the segmentation problem, the standard deviation inside of one certain tissue should be least possible, while the mean value difference between two tissues should be as large as possible. Accordingly, smaller CJV value indicates better bias field correction result.

[2]Available at brainweb.bic.mni.mcgill.ca/brainweb/.

Table 2. Comparison of our methods (LIC and NGLIC) with MICO on segmentation results by average accuracy. The better results are in **bold** (the same for the following tables).

Set No.	MICO	LIC	NGLIC
Set 1	**0.7634**	0.7554	0.7562
Set 2	0.7606	0.7640	**0.7696**
Set 3	0.7211	0.7519	**0.7650**

Table 3. Comparison of our methods (LIC and NGLIC) with MICO on bias correction results by CJV values.

Set No.	Methods		
	MICO	LIC	NGLIC
Set 1	0.6284	0.6020	**0.6014**
	0.6516	**0.6172**	0.6181
	0.6682	**0.6367**	0.6372
	0.5928	**0.5622**	0.5629
	0.6147	0.5840	**0.5839**
	0.6403	**0.6078**	0.6090
Set 2	0.6003	**0.5639**	0.5656
	0.6098	0.5754	**0.5743**
	0.6251	0.5910	**0.5893**
	0.5955	0.5584	**0.5572**
	0.6072	**0.5685**	0.5697
	0.6286	**0.5877**	0.5880

Table 4. CJV Comparison of MICO, LIC and NGLIC on images with non-Gaussian noise.

Set No.	Methods		
	MICO	LIC	NGLIC
Set 3	0.7315	0.6912	**0.6910**
	0.6753	0.6481	**0.6475**
	0.7375	0.6964	**0.6944**
	0.6930	0.6480	**0.6479**

4.2. Results and Analysis

The comparative results on the above 3 sets are shown in Tables 2, 3, and 5. Table 2 presents the segmentation accuracy comparisons, while Tables 3 and 5 illustrate the bias correction results.

As shown in Table 2, MICO performs better than LIC and NGLIC for about 1.05% on *Set 1*, in which only smooth multiplicative bias and Gaussian noise are considered. However, in the more practical situation with complex additive biases and non-Gaussian noises, the proposed LIC and NGLIC perform better than MICO for about 5.74%. As illustrated in Tables 3 and 5, LIC and NGLIC perform better than MICO of all situations. These experiment results indicate the effectiveness of our LIC and NGLIC models. Moreover, on *Set 1* and *Set 2*, the CJV values of LIC and NGLIC are very close, while on *Set 3*, the NGLIC model performs better than the LIC model, shown in Table 3. The results indicate that the introduction of non-Gaussian noise term is necessary for complex noises.

4.3. Real Images Comparisons

In this subsection, we compare the proposed two models with MICO on seven real images that are extracted from [18]. The segmentation and bias correction results are shown in Fig. 2. As shown in this figure, the top three images are distorted by severe biases. All methods can provide satisfactory segmentation results. On the other hand, the bias corrected images of MICO are worse than those of our models. The quantitative results by CJV are shown in Table 5. From this table, we can find that both LIC and NGLIC are better than MICO. Overall, by introducing the non-Gaussian term, the NGLIC model performs better than the LIC model.

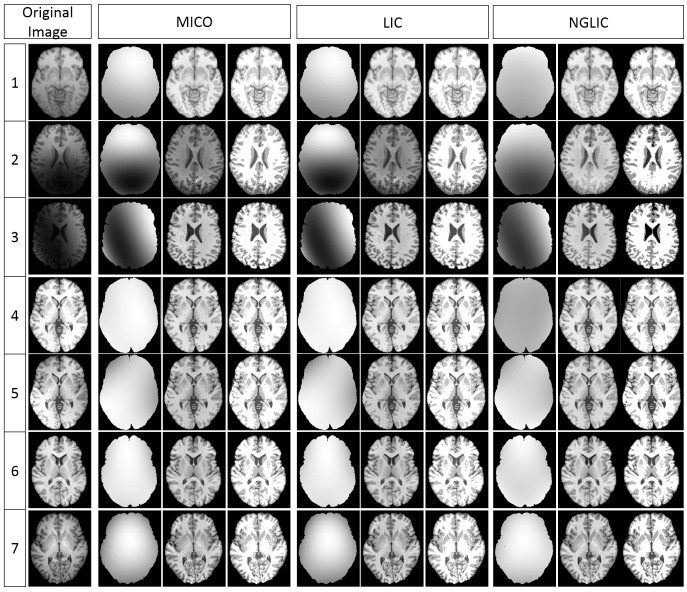

Fig. 2. Experiment results on real images by MICO, LIC and NGLIC models. There are seven images with different intensities of inhomogeneities from up to down. The first column exhibits the original image, and columns $2 \sim 10$ illustrate the results by MICO, LIC, and NGLIC, respectively. In each result, the listed three images are the estimated multiplicative bias field, bias correction image, and segmentation result, respectively.

Table 5. CJV values on images in Fig. 2.

Image No.	Methods		
	MICO	LIC	NGLIC
1	0.5549	0.5524	**0.5512**
2	0.5403	0.5366	**0.5302**
3	0.5362	**0.5342**	0.5519
4	0.5451	0.5351	**0.5096**
5	0.5553	0.5553	**0.5385**
6	0.6072	0.6072	**0.5988**
7	0.5647	0.5641	**0.5563**
Average	0.5577	0.5550	**0.5481**

5. CONCLUSION

In this paper, the new LIC model is proposed to perform image segmentation and bias field correction simultaneously for MR images, which always suffering from intensity inhomogeneities and complex noises. In LIC model, the observed image is assumed to linear transformation of the intrinsic component. The two linear parameters are approximated by constraining them on a subspace, which is composed by spatially smooth functions. We further extend the LIC model to solve complex noise difficulty by introducing the non-Gaussian term, and obtain a new NGLIC model. Comparisons with the MICO model on synthetic and real MR images demonstrate the effectiveness of our models.

6. REFERENCES

[1] David Mumford and Jayant Shah, "Optimal approximations by piecewise smooth functions and associated variational problems," *Communications on pure and applied mathematics*, vol. 42, no. 5, pp. 577–685, 1989.

[2] Xiaohao Cai, Raymond Chan, and Tieyong Zeng, "A two-stage image segmentation method using a convex variant of the mumford–shah model and thresholding," *SIAM Journal on Imaging Sciences*, vol. 6, no. 1, pp. 368–390, 2013.

[3] Yuping Duan, Huibin Chang, Weimin Huang, and Jiayin Zhou, "Simultaneous bias correction and image segmentation via l 0 regularized mumford-shah model," in *2014 IEEE International Conference on Image Processing (ICIP)*. IEEE, 2014, pp. 6–40.

[4] Tony F Chan and Luminita A Vese, "Active contours without edges," *IEEE Transactions on image processing*, vol. 10, no. 2, pp. 266–277, 2001.

[5] Luminita A Vese and Tony F Chan, "A multiphase level set framework for image segmentation using the mumford and shah model," *International journal of computer vision*, vol. 50, no. 3, pp. 271–293, 2002.

[6] Chunming Li, Chiu-Yen Kao, John C Gore, and Zhaohua Ding, "Minimization of region-scalable fitting energy for image segmentation," *IEEE transactions on image processing*, vol. 17, no. 10, pp. 1940–1949, 2008.

[7] Li Wang, Jim Macione, Quansen Sun, Deshen Xia, , and Chunming Li, "Level set segmentation based on local gaussian distribution fitting," in *Asian Conference on Computer Vision*, 2009, pp. 293–302.

[8] K.H.Zhang, H.H.Song, and Lei Zhang, "Active contours driven by local image fitting energy," *Pattern Recognition*, vol. 43, no. 4, pp. 1199–1206, 2010.

[9] Kaihua Zhang, Lei Zhang, Huihui Song, and Wengang Zhou, "Active contours with selective local or global segmentation: A new formulation and level set method," *Image and Vision Computing*, vol. 28, no. 4, pp. 668–676, 2010.

[10] LingFeng Wang, Huai-Yu Wu, and Chunhong Pan, "Region-based image segmentation with local signed difference energy," *Pattern Recognition Letters*, vol. 34, no. 6, pp. 637–645, 2013.

[11] Xiaofeng Wang, De-Shuang Huang, and Huan Xu, "An efficient local chan-vese model for image segmentation," *Pattern Recognition*, vol. 43, no. 3, pp. 603–618, 2010.

[12] LingFeng Wang, Zeyun Yu, and Chunhong Pan, "A unified level set framework utilizing parameter priors for medical image segmentation," *SCIENCE CHINA Information Sciences*, vol. 56, no. 11, pp. 1–14, 2013.

[13] LingFeng Wang and Chunhong Pan, "Robust level set image segmentation via a local correntropy-based k-means clustering," *Pattern Recognition*, vol. 47, no. 5, pp. 1917–1925, 2014.

[14] LingFeng Wang and Chunhong Pan, "Explicit order model for region-based level set segmentation," in *2015 IEEE International Conference on Acoustics, Speech and Signal Processing, ICASSP 2015, South Brisbane, Queensland, Australia, April 19-24, 2015*, 2015, pp. 927–931.

[15] Chunming Li, Rui Huang, Zhaohua Ding, Chris Gatenby, Dimitris Metaxas, and John Gore, "A variational level set approach to segmentation and bias correction of images with intensity inhomogeneity," in *International Conference on Medical Image Computing and Computer-Assisted Intervention*. Springer, 2008, pp. 1083–1091.

[16] Kaihua Zhang, Lei Zhang, and Su Zhang, "A variational multiphase level set approach to simultaneous segmentation and bias correction," in *2010 IEEE International Conference on Image Processing*. IEEE, 2010, pp. 4105–4108.

[17] Lingfeng Wang and Chunhong Pan, "Image-guided regularization level set evolution for mr image segmentation and bias field correction," *Magnetic resonance imaging*, vol. 32, no. 1, pp. 71–83, 2014.

[18] Chunming Li, John C Gore, and Christos Davatzikos, "Multiplicative intrinsic component optimization (mico) for mri bias field estimation and tissue segmentation," *Magnetic resonance imaging*, vol. 32, no. 7, pp. 913–923, 2014.

[19] Abhirup Banerjee and Pradipta Maji, "Rough sets and stomped normal distribution for simultaneous segmentation and bias field correction in brain mr images," *IEEE Transactions on Image Processing*, vol. 24, no. 12, pp. 5764–5776, 2015.

[20] Mei Xie, Jingjing Gao, Chongjin Zhu, and Yan Zhou, "A modified method for mrf segmentation and bias correction of mr image with intensity inhomogeneity," *Medical & biological engineering & computing*, vol. 53, no. 1, pp. 23–35, 2015.

[21] Paul Tseng, "Further applications of a splitting algorithm to decomposition in variational inequalities and convex programming," *Math. Program.*, vol. 48, pp. 249–263, 1990.

[22] Dong Wang, Huchuan Lu, and Ming-Hsuan Yang, "Robust visual tracking via least soft-threshold squares," 2015.